ACS APPLIED MATERIALS & INTERFACES

Research Article

www.acsami.org

Increase in Transgene Expression by Pluronic L64-Mediated Endosomal/Lysosomal Escape through Its Membrane-Disturbing Action

Jianlin Chen,[†,‡] Jing Luo,[†,‡] Ying Zhao,[§] Linyu Pu,[‡] Xuejing Lu,[§] Rong Gao,[†] Gang Wang,*[,‡] and Zhongwei Gu*[,‡]

[†]Key Laboratory for Bio-Resource and Eco-Environment of Ministry Education, Key Laboratory for Animal Disease Prevention and Food Safety of Sichuan Province, College of Life Science, Sichuan University, Chengdu, Sichuan 610064, China

[‡]National Engineering Research Center for Biomaterials, Sichuan University, Chengdu, Sichuan 610064, China

[§]College of Acupuncture and Massage, Chengdu University of Traditional Chinese Medicine, Chengdu, Sichuan 610075, China

ABSTRACT: For efficient transgene delivery and expression, internalized nucleic acids should quickly escape from cellular endosomes and lysosomes to avoid enzymatic destruction and degradation. Here, we report a novel strategy for safe and efficient endosomal/lysosomal escape of transgenes mediated by Pluronic L64, a neutral amphiphilic triblock copolymer. L64 enhanced the permeability of biomembranes by structural disturbance and pore formation in a concentration- and time-dependent manner. When applied at optimal concentration, it rapidly reached the endosome/lysosome compartments, where it facilitated escape of the transfection complex from the compartments and dissociation of the complex. Therefore, when applied properly, L64 not only significantly increased polyethylenimine- and liposome-mediated transgene expression, but also decreased the cytotoxicity occasioned by transfection process. Our studies revealed the function and mechanism of neutral amphiphilic triblock copolymer as potent mediator for safe and efficient gene delivery.

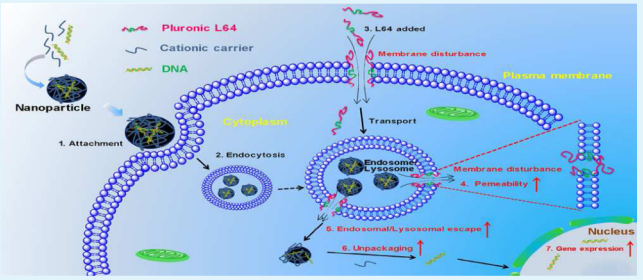

KEYWORDS: *amphiphilic triblock copolymer, PluronicL64, gene delivery, endosomal/lysosomal escape, biomembrane, endocytosis*

INTRODUCTION

Transfer of exogenous genes into cells has been widely used in gene function research, gene therapy, genetic modification of cells and so on.[1−3] Currently, there are two major categories of gene delivery vehicles: viral and nonviral. Viral vectors provide high gene transfer efficiency, but adverse immune responses and random integration of DNA sequences into the host chromosome have limited their therapeutic applications.[4] Synthetic nonviral vectors, such as cationic lipids and polymer, have been investigated as alternatives.[5] However, their gene transfer efficiencies are much lower than those of viral vectors.

To transfer foreign genes into cell nuclei for expression, a gene/vector complex must overcome a series of obstacles, both extracellular and intracellular. The initial set of extracellular barriers includes stability and survival in the circulation, penetration of blood vessels, and binding to the target cells.[6] Upon reaching the targets cells, challenges include achieving internalization across the plasma membrane, escape from endosomes/lysosomes, unpackaging of the complexes, and transport into the nucleus.[7] Internalized gene/vector complexes that become localized within endocytic vesicles can either be transported out of the cell by exocytosis or trafficked into lysosomes where they will be damaged or even destroyed by the hostile environment.[8] Most DNA trapped in lysosomes is degraded and only DNA that escapes into the cytoplasm can survive to reach the nucleus.[9] Endosomal/lysosomal escape is therefore a key step determining the fate of a transgene.

Several strategies have been established to facilitate endosomal/lysosomal escape of transgenes through different mechanisms in nonviral vector-mediated gene delivery. Conjugation of whole, inactivated virus particles with synthetic gene carriers, was shown to enhance transgene expression, possibly due to virus-mediated endosomal escape.[10,11] This approach was impractical owing to the safety concerns raised by the virus. Another approach has been to utilize proteins and peptides derived from viruses,[12,13] bacteria,[14] plants,[15] or animals[16,17] or by incorporating synthetic peptides.[18] Most of them were pH-sensitive amphiphiles that induced the disruption of vesicle membranes at acidic pH.[19] These, however, suffered from the risk of inducing immune reactions upon in vivo applications.[20] A third approach has been to use chemicals, such as polyethylenimine (PEI),[21] polyamidoamines (PAAs),[22] polypropylacrylic acid (PPAA),[23] ammonium chloride,[24] methylamine,[24] chloroquine[25] and poly L-histidine.[26]

Received: January 16, 2015
Accepted: March 19, 2015
Published: March 19, 2015

DOI: 10.1021/acsami.5b00486
ACS Appl. Mater. Interfaces 2015, 7, 7282−7293

These chemicals were considered to have the ability to mediate their own endosomal escape through a "proton-sponge" effect: protonation of the polymer increased the inflow of protons into endocytic vesicles, thereby causing the vesicles to rupture by osmotic swelling. Yet another approach has utilized photochemical disruption of endosomal/lysosomal membranes: after induction by light, certain photosensitizers were found to produce reactive singlet oxygen that destroyed endosomal/lysosomal membranes.[27,28] However, singlet oxygen also had nonspecific side effects on some cellular organelles and enzymes due to its high reactivity.

Lysosomes are important organelles acting as a cellular waste disposal system. They contain acid hydrolases that break down almost all kinds of materials, both intra- and extracellular, such as excess or nonfunctional organelles, proteins, nucleic acids, carbohydrates, lipids and engulfed viruses, bacteria, and particles.[9,29] Consequently, for gene transfer, it is inadvisible to excessively damage lysosomes, although this is usually an effective strategy to increase the transfection efficiency. New strategies are still needed for safe and efficient endosomal/lysosomal escape in transgene delivery and expression.

EXPERIMENTAL SECTION

Materials. Pluronic L64 (PubChem CID: 24751, $EO_{13}PO_{30}EO_{13}$, MW 2900) and branched PEI (MW 25 kDa), Genistein, amiloride, and chlorpromazine were purchased from Sigma-Aldrich (St. Louis, MO). Hematoxylin-eosin (HE) Staining Kit was from Solarbio (Solarbio Science & Technology Co., Ltd., Beijing, China). Texas Red C2-dichlorotriazine (Texas Red), LysoTracker Green/Blue DND-26/22 (LysoTracker), Alexa Fluor 647 NHS Esters (Alexa 647), Dulbecco's modified Eagle's medium with high glucose (4500 mg/L; DMEM), fetal bovine serum (FBS) and OPTI-MEM Reduced Serum Medium (OPTI-MEM) were from Life Technologies Corporation (Invitrogen, Carlsbad, CA). Label ITTracker Intracellular Nucleic Acid Localization Kit (Cy3) was from Mirus Bio Corp. (Mirus, Wisconsin). Dimeric Cyanine Nucleic Acid Stains TOTO-3 dye (TOTO-3) was from Molecular Probes, Inc. (Eugene, Oregon). Cell lysate and the luciferase reporter gene assay kit were from Promega (Madison, WI). BCA protein assay kit was from Pierce (Rockford, IL). Cell counting kit-8 (CCK8) was from Dojindo Laboratories (Kumamoto, Japan). All other chemicals were purchased from Sigma-Aldrich and used as received.

PlasmidspEGFP-C1 (Clontech, TaKaRa Biotechnology Co., Ltd., Dalian, China) encoding the enhanced green fluorescent protein (EGFP) and pGL3-Control (Promega, Madison, WI) containing the modified coding region for firefly (*Photinuspyralis*) luciferase (Luc) were amplified in *Escherichia coli* DH5α and extracted using the PureLink Hipure Plasmid Filter Maxiprep Kit (Invitrogen, Carlsbad, CA). Quality and quantity of purified plasmids were assessed by agarose gel electrophoresis and measurement of the $OD_{260/280}$ in a NanoDrop 2000 (Thermo Fisher, Waltham, MA).

For in vitro experiments, solutions of L64 were prepared at the given concentrations (w/v) in DMEM containing 10% FBS and stored at 4 °C. All buffers were prepared in Milli-Q ultrapure water and filtered (0.22 μm) prior to use.

Cell Culture. Hela (human cervix adenocarcinoma; ATCC No. CCL-2), NIH/3T3 (mouse embryo fibroblast; ATCC No. CRL-1568), C2C12 (mouse muscle myoblast; ATCC No. CRL-1772), H292 (human pulmonary mucoepidermoid carcinoma; ATCC No. CRL-1848) and MDCK (Madin–Darby canine kidney; ATCC No. CCL-34) cell strains were purchased from the Chinese Academy of Science Cellbank (Shanghai, China). Rat bone marrow mesenchymal stem cells (rMSCs) were isolated and cultured as described elsewhere.[30] Cells were grown in DMEM medium containing 4.0 mM L-glutamine, Na pyruvate, 10% FBS, 100 units/mL penicillin, and 100 μg/mL streptomycin (Thermo Fisher, Waltham, MA), and maintained at 37 °C in a 5% CO_2 humidified incubator (Sanyo, Japan).

Observation of Cells by the Time-Lapse Microscopy. HeLa cells were grown in a 24-well glass-bottom culture plate (NEST, Wuxi, China) for 24 h followed by the treatment with L64 at a series of concentrations ranging from 0.02 to 0.20%. Time-lapse images of the cells were recorded automatically at multiple locations on the plate using a Leica AF 700 and DMI6000 B living cell workstation (Wetzlar, Germany) fitted with a 40× Leica objective and an Andor Ixon3 DU885 CCD Camera (Belfast, North Ireland). The microscope was housed in a custom-designed 37 °C chamber with a secondary internal chamber in which the cell culture plate was sustained with humidified 5% CO_2 at 37 °C. A stable focal plane was maintained by an autofocusing system. Differential interference contrast images were obtained every 5 min over a period of 4 h and analyzed using a Leica Microsystems LAS AF6000-Modular System.

Scanning Electron Microscopy Assay. HeLa cells grown on glass coverslips were incubated with L64 at concentrations of 0.02, 0.06, 0.08, or 0.20% for 1 h and then fixed in 2.5% glutaraldehyde/0.1 M phosphate buffer (pH 7.4) for 1 h at 4 °C. After being washed with phosphate buffer three times, cells were dehydrated stepwise in ethanol solutions (30–100%; 10 steps) and stored in amylacetate until use. Cells were then dried in a critical point dryer (Balzers, Germany) and coated with gold nanoparticles. The specimens were examined with an S-4800 scanning electron microscope (Hitachi, Ibaraki, Japan).

Transmission Electron Microscopy Observation. HeLa cells were cultured in a 10 cm plastic dish (Thermo, Waltham, MA) for 24 h and then treated with L64 at 0.06, 0.08 or 0.20% for 1 h, followed by fixation for 24 h at 4 °C in 2.5% glutaraldehyde/4% paraformaldehyde. Fixed cells were gently collected by scraping, suspended in 0.1 M phosphate buffer (pH 7.4) and pelleted in Eppendorf tubes by centrifugation at 1000 g for 5 min. Cell pellets were fixed for 1 h with 2.5% glutaraldehyde and then 1% osmium tetroxide for 1 h at 4 °C. After dehydration in gradient concentrations of ethanol, cells were embedded in Epon-Araldite. Ultrathin sections were cut with a diamond knife in a Leica EM6/UC6 microtome (Balzers, Germany). Thin sections (70 nm) were stained successively with 5% uranyl acetate and 1% lead citrate. Transmission electron microscopy (TEM) observation was performed with a Tecnai G^2 F20 TEM microscope (FEI, Hillsboro, OR) at an accelerating voltage of 200 kV.

Cell-Attached Patch-Clamp Technique. All experiments were performed using the cell-attached mode of the patch-clamp technique. Patch pipettes were pulled from borosilicate glass capillaries (Sutter, CA) using a model P-97 vertical microelectrode puller (Sutter, CA), with opening diameters of 0.5–1.0 μm. HeLa cells were cultured on glass coverslips for 24 h. For patch clamp detection, the pipettes were filled with pipet solution (110 mM KOH, 110 mM Aspartic acid, 1.0 mM $MgCl_2$, 10 mM HEPES, 5.0 mM EGTA, 20 mM KCl; pH 7.4) with resistance values ranging from 2.0 to 5.0 MΩ and backfilled with pipet solution containing different concentrations of L64. When the tip of the pipet was successfully pressed against the cell surface, a giga-ohm seal resistance was established. Cell membrane capacitive currents were recorded by a Multiclamp700B patch-clamp amplifier (Axon, California). The stimulus voltage was 10 mV and a square wave was superimposed on a holding potential of about −60 mV. The output signal of the patch clamp amplifier was analyzed using clampfit.

Hematoxylin–Eosin Staining. HeLa cells were cultured on glass coverslips. After treatment with L64 solutions for 1 h, cells were fixed in 4% paraformaldehyde in 0.1 M phosphate buffer (pH 7.4) for 10 min at 37 °C. Samples were then washed with distilled water three times, stained with 0.5% hematoxylin for 20 min, rinsed, counter-stained in 1% eosin for 10 min, and rinsed again. The cells were observed and photographed using a fluorescent microscope (Nikon eclipse Ti–U, Hitachi, Japan).

L64-Assisted PEI/pDNA Transfection Methods. To optimized the PEI/pDNA transfection method assisted by L64, three different procedures were investigated: (1) LB (L64, before) L64 was added to the medium 2 h before transfection with PEI/pDNA for 4 h. (2) LM (L64, meanwhile) L64 addition was concurrent for the 4 h transfection. (3) LA (L64, after) L64 was added 2 h after the PEI/

DOI: 10.1021/acsami.5b00486
ACS Appl. Mater. Interfaces 2015, 7, 7282–7293

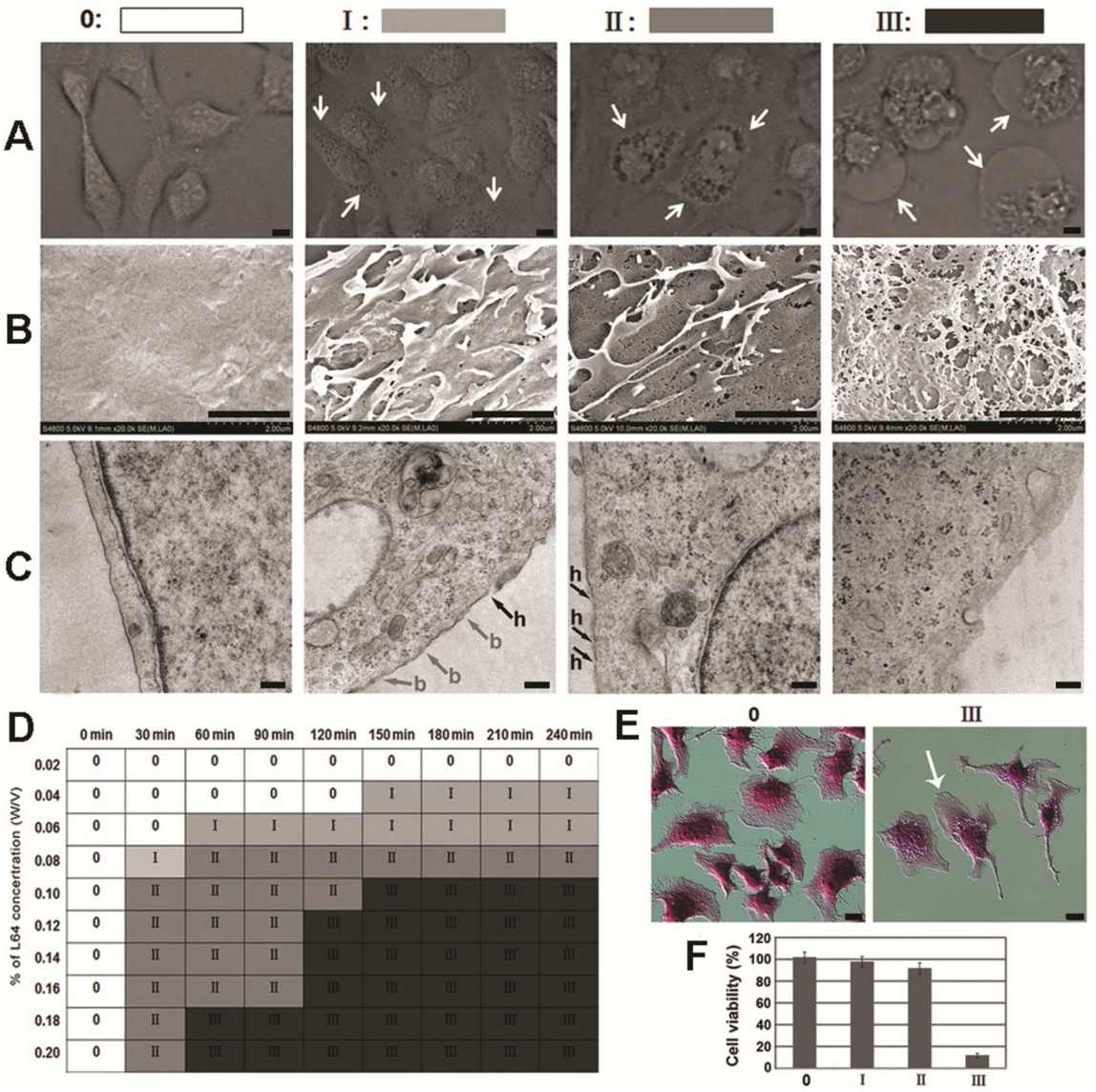

Figure 1. Morphological change of cells treated by Pluronic L64. 0, I, II and III: the 4 typical morphological states of cells. Cell strain: HeLa. (A) Representative cell morphologies for different states visualized by time-lapse microscopy. Scale bar = 10 μm. (B) Cell surface structures visualized by SEM. Cells were treated for 1 h by L64 at different concentrations: 0.02% for state 0; 0.06% for state I; 0.08% for state II; 0.2% for state III. Scale bar = 2.0 μm. (C) Ultrastructure of the cell plasma membrane visualized by TEM. Cells were treated as that in SEM assay. Arrow b, diffuse membrane; arrow h, hole in the membrane. Scale bar = 0.2 μm. (D) Summary of cell states relating to L64 concentration and treatment time. (E) Leakage of intracellular fluid (arrow) in state III by HE staining. Scale bar = 10 μm. (F) Cell viability of different states 48 h after the corresponding treatment.

pDNA transfection and incubated for 2 h. The final concentration of L64 in each method was 0.08% (w/v) in the full medium. PEI and pDNA were combined in OPTI-MEM at an N/P ratio of 10 (except as indicated).

Labeling of L64, PEI, pDNA, and Lysosomes. To label L64, we slowly added 200 μL of Texas Red (10 mg/mL in DMSO) to 2 mL of L64 solution (10 mg/mL in 0.1 M $NaHCO_3$ buffer, pH 9.0). To label PEI, 50 μL Alexa 647 (4 mg/mL in DMSO) was slowly added to 1 mL solution of PEI (2 mg/mL in 0.1 M $NaHCO_3$ buffer, pH 8.3). The mixtures were stirred continuously at room temperature for 1 h in the dark, and the unreacted Texas Red or Alexa 647 was removed by extensive dialysis against distilled water. The labeled PEI and L64 were freeze-dried and stored in −20 °C. Labeling of pDNA with TOTO-3 was carried out according to previously described protocol.[31] To label pDNA with Cy3, 5 μL Cy3 was added to 150 μL pDNA (15 μg), thoroughly mixed and incubated at 37 °C for 1 h. The labeled pDNA was purified by NaCl/ethanol precipitation and centrifugation. To label lysosomes, we incubated cells in a 35 mm dish with 300 μL 75 nM LysoTracker in OPTI-MEM for 30 min. Fluorescent signals were detected by a confocal laser scanning microscopy (CLSM) in a Leica TCS SP5 microscope. (Wetzlar, Germany). The excitation/emission wavelengths (nm) were 588/601 for Texas Red, 642/660 for TOTO-3,550/570 for Cy3, 651/672 for Alexa 647 and 504/511 for LysoTracker.

Intracellular Traffic Analysis of Pluronic L64. HeLa cells were added to a 35 mm glass bottomed dish (Φ = 15 mm; NEST, Wuxi, China) at a concentration of 1×10^4 cells/well, incubated for 24 h and then cultured with 300 μL Texas Red-labeled L64 (0.08% w/v) in fresh OPTI-MEM for 0.5−2 h. For double labeling, lysosomes in the cells were labeled with LysoTracker for 30 min, followed by an additional incubation with Texas Red-labeled L64 for 1 h. Living cells were rinsed three times with PBS (pH 7.4) and observed by CLSM.

Analysis of Endocytic Pathway of Pluronic L64. HeLa cells were added to 6-well plates at a concentration of 1×10^6 cells/well and cultured overnight, followed by the treatment with different endocytic inhibitors (200 μM Genistein, 1.48 mg/mL Amiloride or 20 ug/mL Chlorpromazine) for 30 min at 37 °C. Cells were then incubated for 1 h in fresh medium containing 0.08% Texas Red-labeled

DOI: 10.1021/acsami.5b00486
ACS Appl. Mater. Interfaces 2015, 7, 7282−7293

L64. After incubation, cells were washed with cold PBS three times, harvested, and resuspended in 1 mL PBS. Proportions of fluorescent cells in 1×10^4 cells and their mean fluorescent intensity per cell were measured by fluorescence-activated cell sorting (FACS) in a flow cytometer (BD FACScalibur, BD Bioscience, New Jersey). Data were analyzed by CellQuest software.

Analysis of the Subcellular Localization of PEI and pDNA. The plasmid pEGFP-C1 was labeled with TOTO-3. PEI was labeled with Alexa 647. To observe the intracellular localization of PEI and pDNA in the LA transfection method, we first treated cells with fluorescently labeled PEI/pDNA complex. After 2 h, L64 was added to 0.08% followed by incubation for 1 h, then with an additional treatment with 75 nM LysoTracker for 1 h. Fluorescent signals were recorded by CLSM.

Fluorescence Resonance Energy Transfer (FRET)-based Interaction Assay. FRET was used to evaluate the DNA/PEI interaction. DNA was labeled with Cy3 while PEI with Alexa 647. For FRET measurements in living cells, 6-well plates were seeded with HeLa cells (1×10^6/well) and incubated for 24 h. Cells were transfected with DNA/PEI complex containing 4 μg/well Cy3-labeled DNA and 5 μL/well Alexa 647-labeled PEI (1 mg/mL) using standard or LA transfection protocol. To detect the FRET using the spectral scanning method, the cells were gently harvested by scraping and suspended in 1 mL of PBS. Fluorescent signals in cells were recorded by using a multifunctional microplate reader (Varioskan Flash; Thermo Fisher) with the following parameters: donor channel for Cy3 (excitation/emission, 550/570 nm), acceptor channel for Alexa 647 (excitation/emission, 651/672 nm), and FRET channel (excitation/emission, 550/672 nm). To detect the FRET using the CLSM-based method, we recorded fluorescent signals in cultured cells. We analyzed FRET efficiencies by LAS AF software and calculated them according to the following formula: FRET efficiencies (%) = $(B - A \times \beta - C \times \gamma)/C$, where A, B, and C represent the intensities of the three signals (donor, FRET, and acceptor, respectively), and β and γ are the calibration factors generated by the acceptor and donor, respectively.

Fluorescence-based Evaluation of Gene Delivery Efficiency. To measure the uptake efficiency of fluorescently labeled PEI/pDNA, HeLa cells were added to 6 well plates (1×10^6/well) and incubated to 70−80% confluence. Cells were treated with PEI/pDNA complex containing 4 μg/well TOTO-3 labeled pEGFP-C1 using the LB, LM, and LA transfection methods. Cells were then washed with cold PBS three times, harvested and resuspended in 1 mL of PBS. The proportion of fluorescent cells and their mean fluorescence intensity per cell were measured by FACS using the excitation/emission wavelengths of 642/660 nm.

To evaluate the gene transfection efficiency through EGFP expression, we added NIH/3T3 cells to 24-well plates (2×10^4 cells/well) and allowed them to grow to 70−80% confluence; the cells were then transfected with PEI/pEGFP-C1 complexes (800 ng/well plasmid) at different N/P ratios (1.5, 3, 4, 6, and 10) using the LA transfection protocol. Forty-eight hours (48 h) later, the transfection efficiency was qualitatively evaluated by inverted fluorescent microscopy (Leica DMI 4000B; Wetzlar, Germany). For quantitative determination, the proportion of $EGFP^+$ cells in 1×10^4 cells, and their mean fluorescence intensity per cell were measured by FACS at excitation/emission wavelengths of 488/515 nm.

Luciferase Activity-Based Determination of Gene Delivery Efficiency. To quantitatively analyze the gene transfection efficiency via luciferase expression, cells transfected with pGL3-control 48 h previously were washed with cold PBS and lysed with 1× lysis reporter buffer (Promega). Cell debris was then removed by centrifugation at 12 000g for 5 min at 4 °C, and total protein concentrations of the supernatants were determined using the BCA Protein Assay Kit (Pierce, Rockford, IL), with bovine serum albumin (BSA) as a standard. Luciferase activity was measured in a multifunctional microplate reader. Gene transfection efficiency was determined as luciferase activity, normalized to total protein concentration and calculated as relative light units per milligram of total protein (RLU/mg protein).

Cell Cytotoxicity Assay. The cytotoxicity of the LB, LM, and LA transfection procedures for cultured cells was evaluated by CCK-8 assay. HeLa, NIH/3T3 and MDCK cells were added to 96 well plates (8.0×10^3 cells/well) and cultured to 70−80% confluence. PEI/pDNA complexes were added to each well according to the LB, LM and LA procedures as described. After 24 h, 10 μL CCK-8 solutions (5 mg/mL in PBS) were added to each well for an additional 2 h of incubation. Absorbances were measured by a multifunctional microplate reader (Varioskan Flash; Thermo Fisher) at 490 nm. The cell viability was calculated according to the following formula: cell viability (%) = $[(A_{sample} - A_{blank})/(A_{control} - A_{blank})] \times 100$, where A_{sample}, $A_{control}$, and A_{blank} represent the absorbance values of transfected cells, untransfected cells, and medium alone, respectively.

Statistical Analysis. All experiments were conducted in triplicate, and data are presented as means ± SD from at least three independent samples. Statistical analyses were determined by analysis of variance tests (ANOVA) using the software of GraphPad Prism 6.0. Statistical comparisons between groups were made using the Student's t test. Values of $P < 0.05$ were considered to be statistically significant.

RESULTS

L64 Influences the Structure and Permeability of Cell Membranes. When HeLa cells were treated with a series of concentrations of Pluronic L64 for 4 h, dynamic changes in cell morphology were observed by time-lapse microscopy (Figure 1A). Treated cells showed four typical morphologies, classified as states 0, I, II, and III (Figure 1). Cells treated with low L64 concentrations for a short time (0.02% for 4 h, 0.04% within 2 h and 0.06% within 0.5 h) exhibited state 0 (Figure 1D); i.e., indistinguishable from untreated normal cells. With the increase of L64 concentration and treatment time, however, pits of different sizes appeared on the cell surface (states I and II). In state III, large globules had formed and cell contents were condensed (Figure 1A). The globules were further confirmed to be the intracellular fluid leaked out through the plasma membrane (Figure 1E). The cell surface morphologies of the four states were further visualized by SEM: no significant change was observed in the state 0; formation of pits with increased number, and diameter was seen in the states I and II with severe damage apparent in the state III (Figure 1B).

To determine if there were actual holes penetrating the cell membranes, wee visualized ultrastructural changes in plasma membranes in cell sections by TEM (Figure 1C). After 1 h of treatment with 0.02% L64, the cell membrane maintained normal integrality (state 0). Upon increase to 0.06% L64, diffuse regions (arrow b) and holes penetrating the membrane (arrow h) were also observed (state I). At 0.08% L64, the whole plasma membrane became blurry and indistinct and was disrupted by an increased number of holes (state II). The plasma membrane was almost destroyed by the 0.2% L64 treatment, with disappearance of the membrane structure (state III).

Because cells were able to grow normally in states 0, I ,and II but could not survive in state III, we considered L64 at a concentration of 0.08% generated state II (Figure 1F) to be the most suitable concentration for safe and efficient treatment of cells. Altogether, the results revealed that Pluronic L64 induced morphological changes in cells in a concentration- and time-dependent manner.

Disturbance of plasma membrane structure by L64 should affect capacitive currents across the membrane. To investigate this point, the cell-attached patch-clamp technique was used to continuously record the capacitive currents within the patch membranes after the addition of L64. The patch membranes were first charged at 10 mV for 10 ms (Figure 2A), and the

DOI: 10.1021/acsami.5b00486
ACS Appl. Mater. Interfaces 2015, 7, 7282−7293

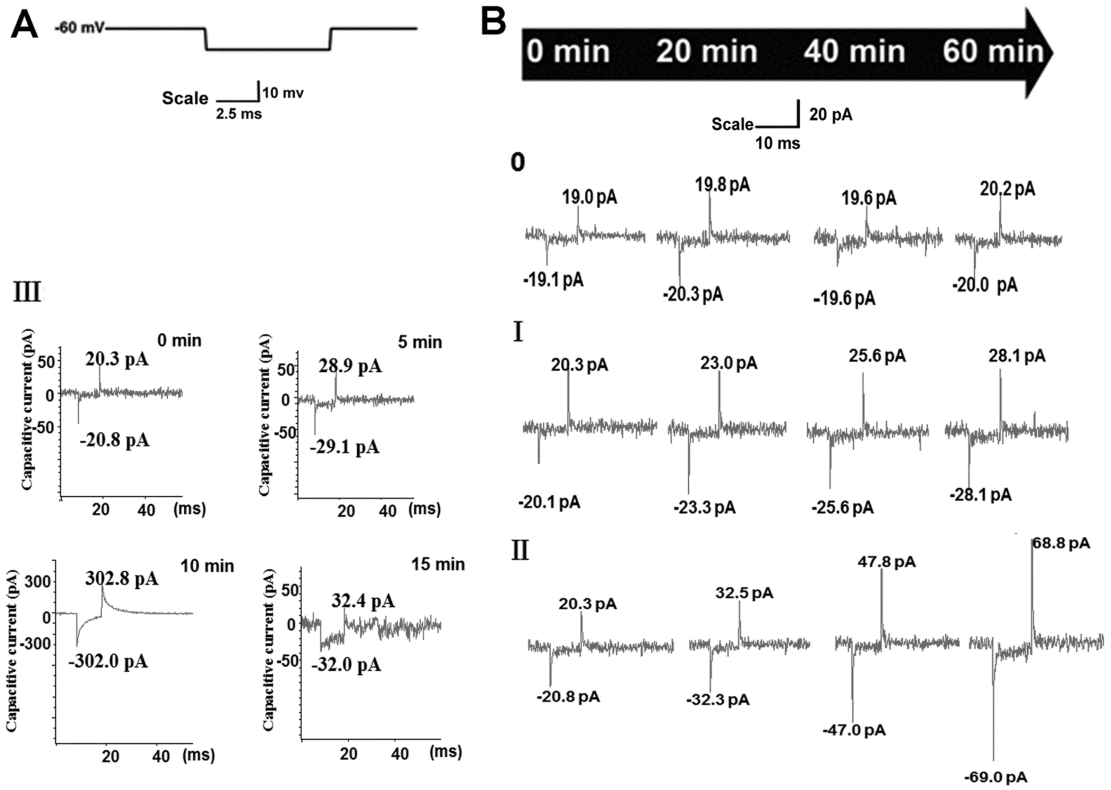

Figure 2. Representative records of the capacitive currents in L64-treated cell membranes by the cell-attached patch-clamp technique. Cell strain: HeLa. $N = 6$. (A) The charging course on the patch of membrane. Voltage, 10 mV; time, 10 ms; holding potential, −60 mV. (B) Capacitive currents through the patch membranes treated with (0) 0.02, (I) 0.06, (II) 0.08, and (III) 0.20% Pluronic L64. A giga-ohm seal was established at 0 min and the capacitive currents were continuously recorded thereafter.

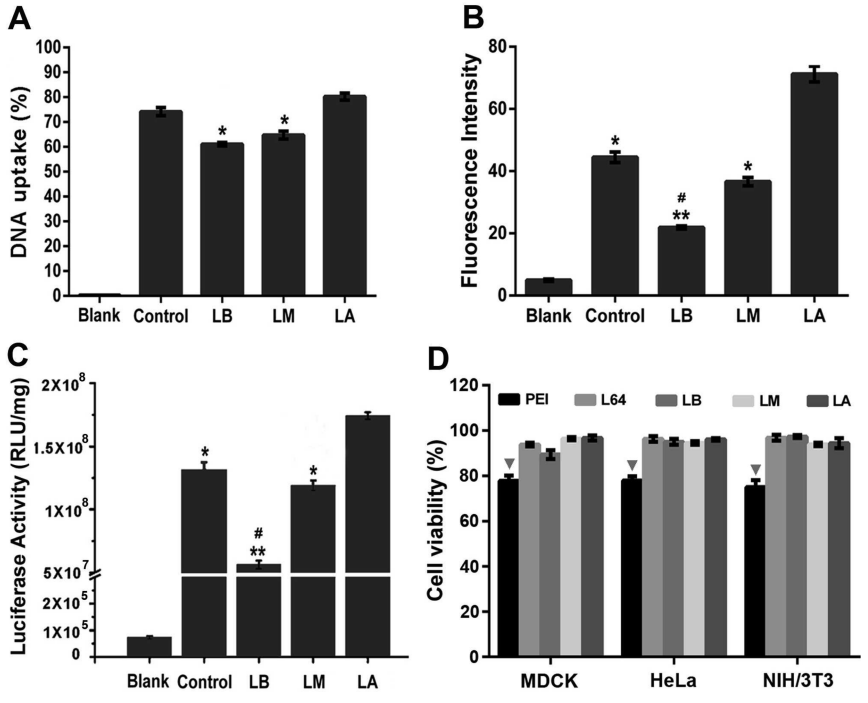

Figure 3. Gene delivery efficiency by different methods and cell viability. Blank: without transfection. Control: PEI/pDNA standard transfection. pDNA: pGL3-control. LB, LM, and LA: L, L64; B, before PEI/pDNA administration; M, meanwhile with PEI/pDNA administration; A, after PEI/pDNA administration. Cells for transfection: HeLa. (*) $P < 0.05$ vs LA. (**) $P < 0.01$ vs LA. (#) $P < 0.05$ vs Control and LM. (A) Percent of fluorescent cells and (B) average fluorescence intensity in each cell uptaking fluorescently labeled pDNA/PEI, analyzed by FACS. In the PEI/DNA complex, DNA was fluorescently labeled with TOTO-3. Plate: 6-well format. $N = 3$. (C) Transfection efficiency measured by luciferase activity. Plate: 96-well format. $N = 6$. (D) Cell viability assayed by CCK-8. Plate: 96-well format. $N = 6$. (▼) $P < 0.05$ vs others.

DOI: 10.1021/acsami.5b00486
ACS Appl. Mater. Interfaces 2015, 7, 7282−7293

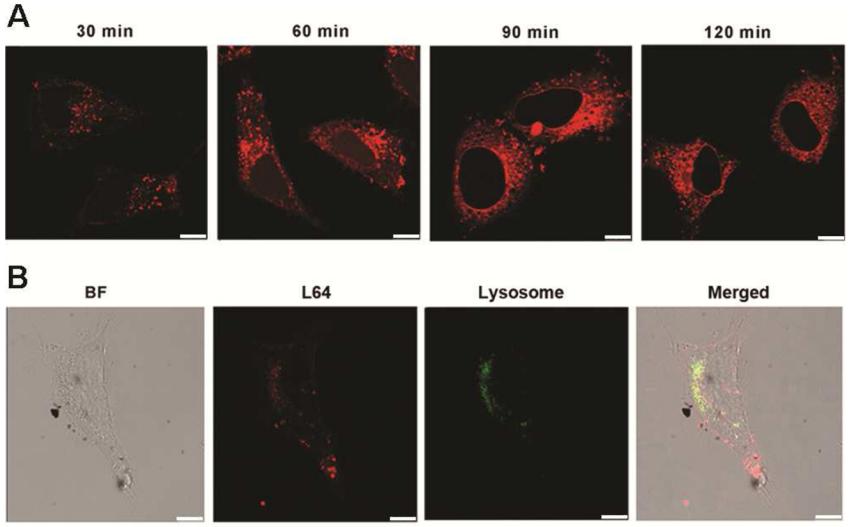

Figure 4. Intracellular traffic and subcellular location of L64 in HeLa cells. (A) Timelapse photographs of the intracellular traffic of L64. Cells were incubated with Texas Red-labeled L64 for different times and photographed by CLSM. Scale bar = 10 μm. (B) Co-localization of L64 with intracellular lysosomes. Cells were labeled with LysoTracker for 30 min followed by Texas Red-labeled L64 for 1 h, and observed by CLSM. Scale bar = 10 μm.

capacitive currents were recorded for 1 h (Figure 2B). The mean value of currents through 0.02% L64-treated cell membranes (state 0) was 19.6 pA and was sustained at this level over the 1 h recording period, indicating that the plasma membrane was little affected. When cells were treated with 0.06% L64 (state I), the currents increased slightly. At 0.08% L64 (state II), increases in capacitive currents became faster and stronger. At 0.2% L64 (state III), however, the currents sharply increased to 302 pA within 10 min, then suddenly fell to 32 pA 5 min later, indicating that the patch membranes were destabilizing rapidly and damaged so severely that the electrodes became separated from the membranes soon after. The results indicated that the membrane permeability was affected by L64 in a concentration-dependent manner within a certain range of concentrations. The increased permeability of the cell membrane was additionally confirmed by the leakage of cytosol (Figure 1E).

Increase of PEI/DNA Transfection by L64 is Not Due to the Disturbance on Cell Plasma Membranes. Increases in permeability and development of pores in L64-treated cell membranes might be expected to establish a more efficient gene delivery method. However, the results showed that this was not the case. When 0.08% L64 was added 2 h before transfection (method indicated as LB), the internalization of PEI/DNA was inhibited (Figure 3A, B; LB vs Control, $P < 0.05$) indicating that the disturbance of plasma membrane by L64 might have interfered with the endocytic function of the membrane, thereby inhibiting expression of the transgene (Figure 3C; LB vs Control, $P < 0.05$).

When L64 was added 2 h after PEI/DNA transfection (method indicated as LA), the internalization of the complexes was not influenced by L64 (Figure 3A; LA vs Control). Theoretically, the amount of internalized DNAs in LA cells should not be higher than that in control cells because the internalization process in the LA method was interfered by L64 for 2 h. However, the average fluorescence intensity of internalized DNA in LA cells was significantly higher than that in the other groups, and consequently the transgene expression was greatly increased (Figure 3B,C; LA vs others, $P < 0.05$). These results indicated that events separate from internalization had taken place in the cytoplasm, resulting in L64 having a positive effect on the survival of internalized plasmid DNA (pDNA) in LA cells permitting it to function efficiently in the subsequent cascade events of nuclear transport, gene transcription, and translation.

When L64 and PEI/pDNA were added to cells simultaneously (method LM), there was no apparent effect on the PEI/pDNA internalization and transgene expression (Figure 3A–C; LM vs Control). This may be due to a balance between L64's negative and positive effects on internalization and subsequent intracellular events, respectively.

It is of note that the addition of L64 can significantly reduced the cytotoxicity of PEI/pDNA transfection in several cell strains, regardless of the transfection methods (Figure 3D).

L64 Facilitates the Dissociation of PEI/pDNA Complex and Endosomal/Lysosomal Escape of pDNAs in the Cells. Because disturbance of the cell plasma membrane by L64 had a negative effect on gene transfer into cells, it appeared that L64 produced a positive effect during the subsequent intracellular events since the internalized pDNA and transgene expression were increased. Intracellular traffic of L64 was therefore investigated. As shown in Figure 4A, the Texas Red-L64 molecules became increasingly internalized within the cell cytoplasm over a 2 h observation period. The labeled L64 accumulated rapidly in the cytoplasm, but little or none was seen to enter the nucleus. The internalized L64 molecules appeared to aggregate in the lysosomes. To confirm this, we specifically labeled lysosomes, and results showed that most of the internalized L64 molecules did indeed localize within lysosomes (Figure 4B).

The endocytic pathways for intracellular entry of particles and solutions may determine their intracellular traffic and final localization, which thereby influence their fate and function.[32,33] To explore the endocytic pathways for L64, endocytosis inhibitor Chlorpromazine, genistein, and amiloride were employed to block clathrin-, caveolin- and macropinocytosis-mediated endocytosis, respectively.[34,35] Results showed that chlorpromazine inhibited the cellular uptake of L64 by 15.6%

DOI: 10.1021/acsami.5b00486
ACS Appl. Mater. Interfaces 2015, 7, 7282–7293

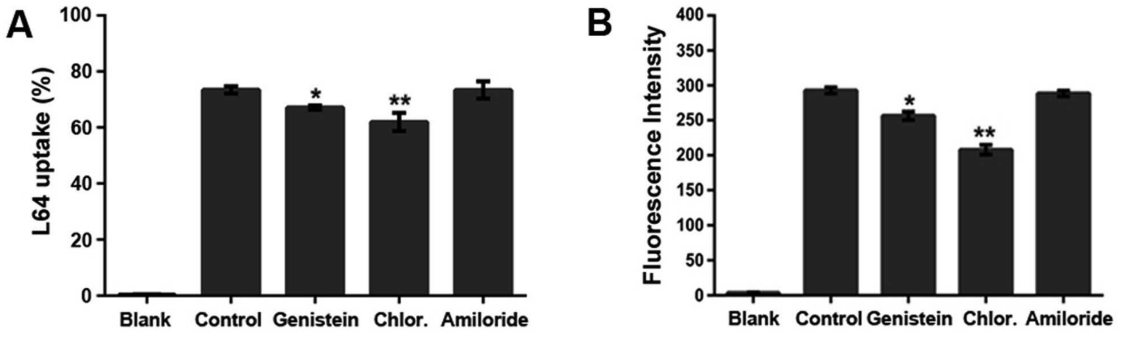

Figure 5. Influence of L64 internalization by endocytosis inhibitors in HeLa cells. Cells were treated with different inhibitors for 0.5 h followed by 0.08% Texas Red-labeled L64 for 1 h. Blank: untreated cells. Control: treated with 0.08% Texas Red-labeled L64 only. Chlor.: chlorpromazine. (A) Proportions of fluorescent cells and (B) the mean fluorescent intensity per cell were measured by FACS. (*) $P < 0.05$, (**) $P < 0.01$ vs Control.

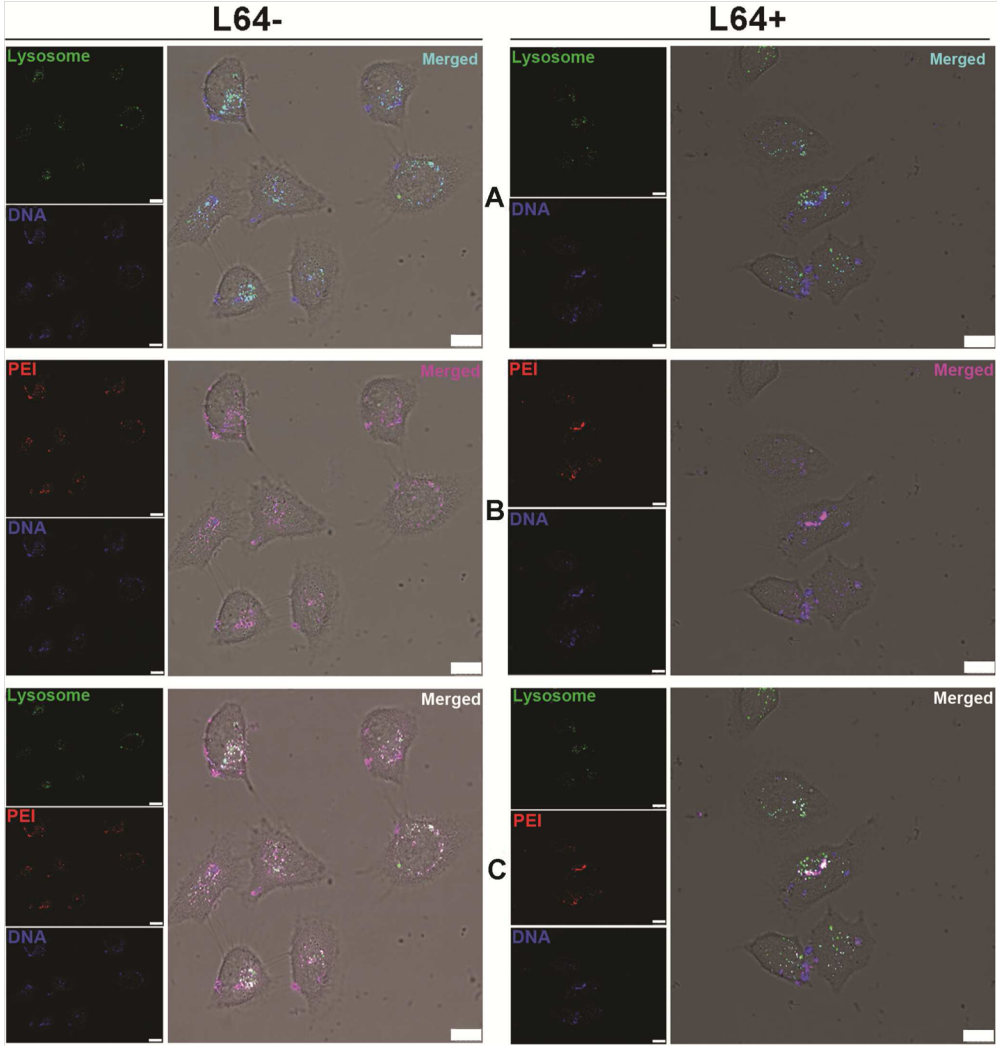

Figure 6. Effect of co-localization of PEI, DNA, and lysosome by L64 in HeLa cells. Cells were treated with fluorescently labeled PEI/pDNA complex for 2 h, followed by 0.08% L64 for 1 h and then LysoTracker for 1 h. The fluorescent signals were recorded by CLSM. Scale bar = 10 μm. The merged signals were (A) cyan for lysosome/DNA, (B) purple for PEI/DNA and (C) white for lysosome/PEI/DNA (L64−, merged), which were decreased by the addition of L64, whereas the original signals (green for lysosome, blue for DNA, and red for PEI) were increased (L64+, merged).

(Figure 5A) as well as the average fluorescence intensity of internalized L64 (decreased by 28.97%; Figure 5B). Genistein also had an inhibitory effect on the endocytosis of L64, while amiloride displayed little inhibition ability (Figure 5). The results revealed that L64 molecules entered the cells through the clathrin-mediated endocytic pathway and partly through the caveolin-mediated pathway. Both pathways begin from the engulfment of cargoes by the plasma membrane, forming the intracellular vesicles. For clathrin-mediated endocytosis, the clathrin-coated vesicles are orderly transferred to the early

DOI: 10.1021/acsami.5b00486
ACS Appl. Mater. Interfaces 2015, 7, 7282−7293

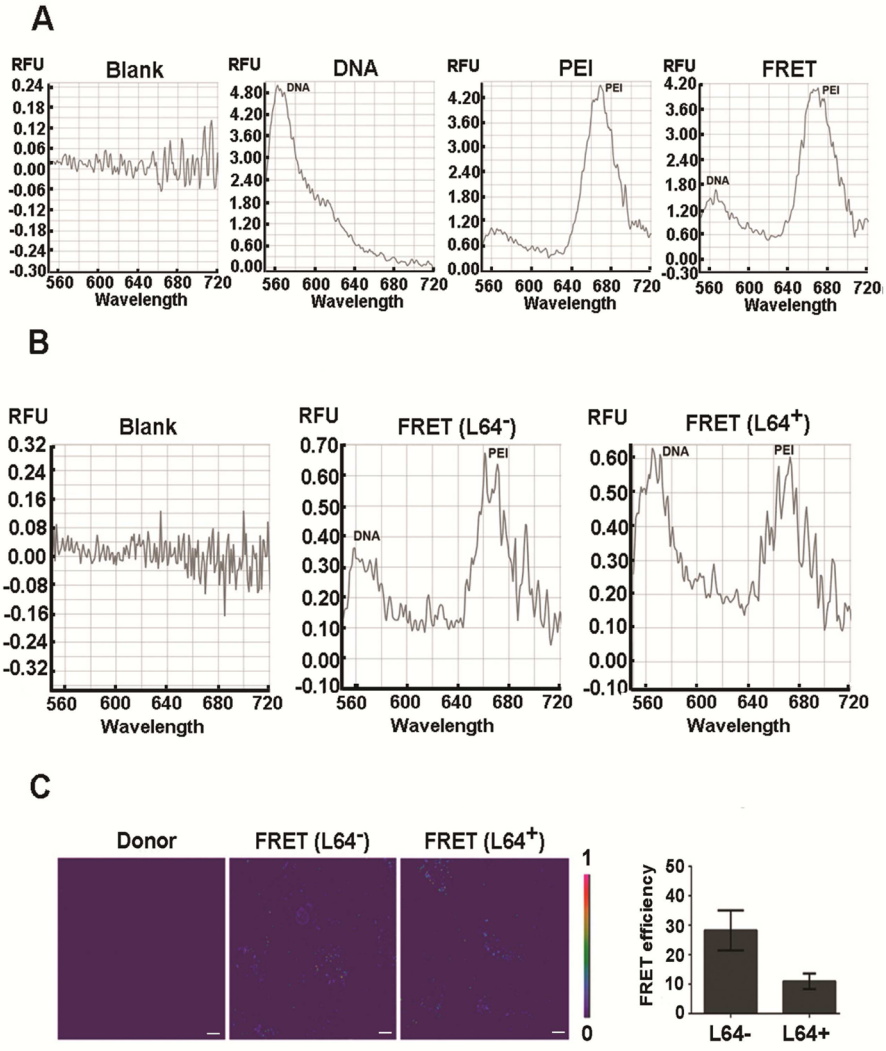

Figure 7. FRET-based analysis of the dissociation of PEI/pDNA complex in HeLa cells. (A) Confirmation of the in vitro FRET effect between PEI and pDNA by spectral scanning. (B) Detection of FRET in cells by spectral scanning. (C) Detection of FRET efficiency in cells by CLSM. Donor: cells were transfected with PEI/DNA complex wherein only the DNA was labeled by Cy3. Scale bar = 10 μm.

endosome, late endosome, and lysosome.[35,36] For caveolin-mediated endocytosis, part of the intracellular vesicles is also transferred to lysosome.[35] Previous studies have reported that the branched PEI utilized both clathrin- and caveolin-mediated endocytosis pathways.[37,38]

L64 and PEI share the same endocytic pathways, implying that there might be interaction between the molecules during the intracellular trafficking process. For example, the membrane-disturbing function of L64 might increase the permeability of endosomal/lysosomal membranes so that the encapsulated PEI/pDNA cargoes could escape more easily, leading to increased gene delivery and expression. Visualization of the co-localization of fluorescently labeled lysosome, pDNA, and PEI molecules in cells with/without the addition of L64 showed that the merged signals (i.e., co-localized components) were dominant in L64-free cells (Figure 6, L64−), whereas the signals of the individual components were increased by the addition of L64 (Figure 6, L64+). It could be concluded that the addition of L64 did facilitate the separation of DNA from lysosomes (Figure 6A) and PEI (Figure 6B), and promote the detachment of DNA and PEI (Figure 6C). The accelerated detachment of the three fluorescent signals indicates the escape of DNA and PEI from lysosomes, which may be due to the disturbance of the lysosomal membrane by L64.

Detachment of the PEI/DNA complex was further quantitatively evaluated by the fluorescence resonance energy transfer (FRET)-based assays. In a cell-free system, when DNA and PEI were combined, the PEI peak was dominant, indicating that an efficient FRET had occurred between the DNA and PEI molecules (Figure 7A). In living cells, the dominance of the PEI peak was still obvious, confirming the existence of a FRET event between the two molecules (Figure 7B; L64$^-$); however, when L64 was added, the DNA peak sharply increased to the same level as PEI, demonstrating that the FRET efficiency was greatly decreased (Figure 7B; L64+). The interruption of FRET by L64 was also confirmed by confocal laser scanning microscopy (CLSM). When L64 was added, the FRET efficiency was reduced from ∼28 to ∼10% (Figure 7C), revealing that a large proportion of PEI/DNA complexes were dissociated. These data confirmed that unpackaging of PEI/DNA complexes was reduced by L64.

Optimization of L64-Assisted Gene Transfection Method. To optimize conditions for L64-assisted PEI/pDNA transfection by the LA method (L64 was added 2 h

DOI: 10.1021/acsami.5b00486
ACS Appl. Mater. Interfaces 2015, 7, 7282−7293

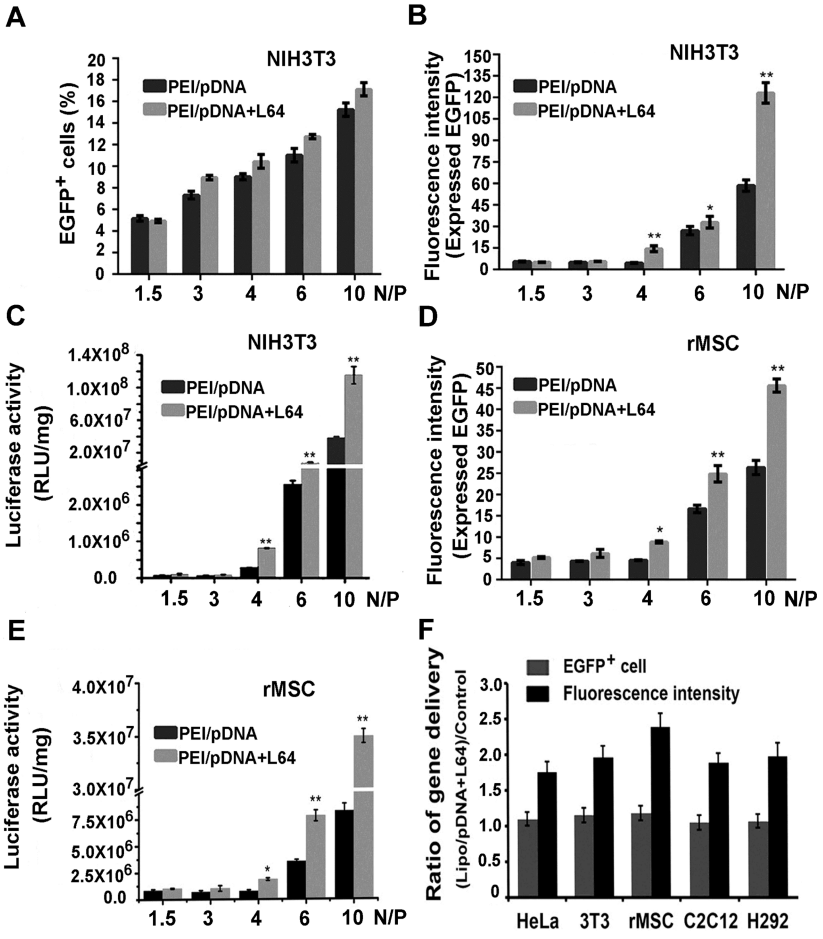

Figure 8. L64-assisted gene delivery in different cell strains. (A–E) Optimization of L64-assisted PEI/pDNA transfection in (A–C) NIH/3T3 cells and (D, E) rMSC cells. PEI/pDNA: PEI standard transfection method. PEI/pDNA + L64: cells were transfected with PEI/pDNA and L64 using the LA method. (*) $P < 0.05$ and (**) $P < 0.01$ vs PEI/pDNA. $N = 3$. (A) Transfection efficiency evaluated by the percentage of EGFP-expressing cells detected by FACS. (B and D) Average fluorescence intensity per cell in EGFP-expressing cells detected by FACS. (C and E) Transfection efficiency evaluated by luciferase activity assay. (F) Ratio of gene transfection efficiency and expression between the (Lipo/pDNA + L64) and control methods. Lipo/pDNA + L64: cells were treated with Lipofectamine2000/pEGFP-C1 and then L64 using the LA method. Control: Lipofectamine2000 standard transfection method. The transfection efficiency was evaluated by measuring the proportion percentage of EGFP-expressing cells. The gene expression level was evaluated by determining the average fluorescence intensity per cell in EGFP-expressing cells detected by FACS. $N = 3$.

after PEI/DNA transfection), the effect of the N/P ratio, the most important parameter in PEI/pDNA transfection was evaluated. With the NIH/3T3 cell line, the proportion of cells expressing EGFP at each N/P value tested, was not improved by the addition of L64 (Figure 8A), indicating that the internalization efficiency was not increased. However, at N/P ratios above 3, the addition of L64 significantly increased the expression of EGFP and luciferase (Figure 8B,C). The N/P ratio of 10 was also the optimum parameter for the L64-assisted LA method, the same as in PEI/pDNA standard transfection. At an N/P ratio of 10, the gene expression level was increased to 2-fold for EGFP and 3-fold for luciferase. The increase in transgene expression was further confirmed in primary rMSC cells (Figures 8D,E), indicating that in these cells as well, L64 was beneficial to the intracellular events for transgene expression, that is, to endosomal/lysosomal escape and unpackaging of the complex. This was in line with previous results.

We think that this method should also be applicable for cationic liposome-mediated gene transfer because liposomes have the analogous structure to biomembranes, so that they would be disturbed by L64, leading to accelerated escape and/or detachment of DNA from liposomes. The results showed that the transgene expression level was significantly increased in several cell strains with the addition of 0.08% L64 after a 2 h transfection by Lipofectamine2000/pEGFP-C1, whereas the entry of the lipoplex into cells was not influenced (Figure 8F).

Altogether, the optimal L64-assisted method was to add L64 at a final concentration of 0.08% after the PEI/pDNA (N/P = 10) or Lipofectamine2000/pDNA transfection for 2 h and then incubate for an additional 2 h. It can greatly increase the transgene expression level and reduce the cytotoxicity.

DISCUSSION

In nonviral vector-mediated gene delivery cases, the internalized gene/vector complexes must escape quickly from the endocytic vehicles to avoid being trapped in lysosomes and destroyed by the hostile environment. The endosomal/lysosomal escape process can be considered a protective mechanism because extensive damage and disruption of lysosomes can have a deleterious effect on the cell. This may be why certain gene delivery materials, such as "proton-sponge" materials, photosensitizers, proteins, and peptides, present unacceptable degrees of cytotoxicity. In contrast, the novel

DOI: 10.1021/acsami.5b00486
ACS Appl. Mater. Interfaces 2015, 7, 7282–7293

strategy described in this study provides a solution for the conflict between efficiency and safety in, at least, PEI- and liposome-mediated gene delivery.

Pluronics have been widely used as pharmaceutical adjuvants.[39] Previous studies also showed that Pluronics such as L64,[40] P85,[41] and F127[42] increased transgene expression in rodent skeletal muscle. Among these, Pluronic L64 was the most efficient and stable one.[40] Until the present work, the mechanism of enhancement of transgene expression by Pluronics has been simply a matter for speculation.[43] It has been reported that Pluronics L64[40] and P85[41] can activate the NF-κB signal pathway and thereby increase the transcription of transgene. But we think it is just a part of molecular mechanisms underlying Pluronics' function. Our ongoing work is in analyzing the regulation network of gene transcription activated by Pluronic L64 in target cells using DNA microarrays, bioinformatics and other molecular biology technologies so as to reveal the overall mechanisms of L64 on the activation of gene expression in the cells. Studies using models of artificial lipid membranes have shown that Pluronic copolymers produced changes in membrane microviscosity and the formation of pores,[44−46] but comparable work based on cell membranes had not been done. Because the characteristics of cell membranes are much more complex than those of model lipid membrane, results obtained with the latter cannot necessarily be projected to explain what occurs in biological membranes. Therefore, we performed the exploration on living cell membranes. This provided the impetus for the present investigation.

Pluronics are a series of amphiphilic copolymers consisting of hydrophilic poly(ethylene oxide) (PEO) and hydrophobic poly(propylene oxide) (PPO) blocks arranged in a PEO−PPO-PEO triblock.[42,47] Members of the series are characterized by differences in the proportions of PEO and PPO, hydrophilic−lipophilic balance (HLB) and critical micellar concentration (CMC).[42,43] As amphiphilic triblock copolymers, Pluronics share a hydrophilic−hydrophobic−hydrophilic structure with the phospholipid bilayer in biomembranes such as the plasma and organelle membranes. Theoretically, driven by the hydrophilic−hydrophobic effect, the amphiphilic triblock copolymers have been considered to interact with the phospholipid pairs in cell membranes, resulting in alterations of membrane structure and function which might facilitate the DNA entrance into cells. In the present work, we found that Pluronic L64 did influence the structure and permeability of plasma membrane of cultured cells (Figures 1 and 2), but also that the endocytic function of the membrane was disturbed, leading to inhibition of L64 internalization and transgene expression (Figures 3A−C; LB and LM vs Control). The finding of intracellular localization of L64 in lysosomes provides suggestive clues (Figure 4). The finding that L64 shared endocytic pathways with PEI/pDNA particles also suggested the final co-localization of these molecules in lysosomes (Figure 5). The internalization of L64 occurred rapidly (Figure 4A). Upon internalization in cells after the endocytosis of PEI/pDNA, L64 at optimal concentration exerted influence on the biomembranes of endosomes/lysosomes during the trafficking process, thereby increasing their permeability instead of disrupting the structure, resulting in accelerated escape of PEI/pDNA from endosomes/lysosomes and unpackaging of PEI/pDNA complex (Figures 6 and 7). The discovery of the mechanism inspired us to establish L64-assisted PEI- and liposome-mediated gene transfection methods for different cell lines (Figure 8). We think that the method can be applied to other cationic gene delivery copolymers, which mainly utilize the clathrin-mediated endocytosis pathway and thereafter undergo the ensosome-lysosome transport.[37]

The present study has shown that the amphiphilic triblock copolymer L64, which shares a similar structure with biomembranes, had the ability to increase transgene expression through a unique mechanism. Several key parameters, such as the size and architecture of the copolymer, length and ratio of their component blocks, influence the function of Pluronics, which may be the reason only some are capable of increasing transgene expression.[40−42] The activity of Pluronics is based mainly on their disturbance effects on biomembranes, so the copolymers should be rationally designed regarding to the architectures of biomembranes. We designed another kind of amphiphilic triblock copolymer, which had the hydrophobic−hydrophilic−hydrophobic structure, the reverse of that of L64, and showed that it had better intramuscular performance than L64.[48] We think that the function of both kinds of copolymers may be improved by optimizing the above-mentioned key parameters. The copolymers showed potential for the establishment of more powerful method for in vitro and in vivo gene delivery and expression.

CONCLUSION

The internalized transfection complexes should escape from the endocytic vehicles as soon as possible to avoid being transported to lysosomes or being trapped in lysosomes for a long time. For nonviral vector-mediated gene delivery, the endosomal/lysosomal escape process should be rationally designed to protect the organelles from being severely damaged. Here, the study presented a new resolution for safer and more efficient endosomal/lysosomal escape of transgene and the dissociation of the transfection complexes. The addition of Pluronic L64 after a 2 h transfection of polyplex or lipoplex greatly increased the expression of transgene in different cell lines, which was a benefited of the moderately structure-disturbing effects on biomembranes of endocytic vehicles by L64 at optimized concentration. The study showed that the neutral amphiphilic triblock copolymers had potent and safe function on endosomal/lysosomal escape through their unique properties.

AUTHOR INFORMATION

Corresponding Authors

*Tel./Fax: +86 28 85412923. E-mail: wgang@scu.edu.cn.
*Tel.: +86 28 85410336. Fax: +86 28 85410653. E-mail: zwgu@scu.edu.cn.

Notes

The authors declare no competing financial interest.

ACKNOWLEDGMENTS

This work was supported by the National Basic Research Program of China (No. 2011CB606206), the National Natural Science Foundation of China (No. 313709, 51133004, 81361140343), and the National Support Program of Science and Technology (No. 2012BAI17B06).

REFERENCES

(1) Zhang, S.; Zhao, B.; Jiang, H.; Wang, B.; Ma, B. Cationic Lipids and Polymers Mediated Vectors for Delivery of siRNA. *J. Controlled Release* **2007**, *123*, 1−10.

DOI: 10.1021/acsami.5b00486
ACS Appl. Mater. Interfaces 2015, 7, 7282−7293

(2) Colosimo, A.; Goncz, K.; Holmes, A.; Kunzelmann, K.; Novelli, G.; Malone, R.; Bennett, M.; Gruenert, D. Transfer and Expression of Foreign Genes in Mammalian Cells. *Biotechniques.* **2000**, *29*, 314−331.
(3) Sun, N.; Liu, Z.; Huang, W.; Tian, A.; Hu, S. The Research of Nanoparticles as Gene Vector for Tumor Gene Therapy. *Crit. Rev. Oncol. Hematol.* **2014**, *89*, 352−357.
(4) Bessis, N.; GarciaCozar, F.; Boissier, M. Immune Responses to Gene Therapy Vectors: Influence on Vector Function and Effector Mechanisms. *Gene Ther.* **2004**, *11*, S10−S17.
(5) Mintzer, M. A.; Simanek, E. E. Nonviral Vectors for Gene Delivery. *Chem. Rev.* **2009**, *109*, 259−302.
(6) Pouton, C. W.; Seymour, L. W. Key Issues in Non-viral Gene Delivery. *Adv. Drug Delivery Rev.* **1998**, *34*, 3−19.
(7) Davis, M. E. Non-Viral Gene Delivery Systems. *Curr. Opin. Biotechnol.* **2002**, *13*, 128−131.
(8) De Duve, C. The Lysosome Turns Fifty. *Nat. Cell Biol.* **2005**, *7*, 847−849.
(9) Settembre, C.; Fraldi, A.; Medina, D. L.; Ballabio, A. Signals from the Lysosome: A Control Centre for Cellular Clearance and Energy Metabolism. *Nat. Rev. Mol. Cell Biol.* **2013**, *14*, 283−296.
(10) Wagner, E.; Zatloukal, K.; Cotten, M.; Kirlappos, H.; Mechtler, K.; Curiel, D. T.; Birnstiel, M. L. Coupling of Adenovirus to Transferrin-Polylysine/DNA Complexes greatly Enhances Receptor-Mediated Gene Delivery and Expression of Transfected Genes. *Proc. Natl. Acad. Sci. U.S.A.* **1992**, *89*, 6099−6103.
(11) Cotten, M.; Wagner, E.; Zatloukal, K.; Phillips, S.; Curiel, D. T.; Birnstiel, M. L. High-Efficiency Receptor-Mediated Delivery of Small and Large (48 Kilobase Gene Constructs Using the Endosome-Disruption Activity of Defective or Chemically Inactivated Adenovirus Particles. *Proc. Natl. Acad. Sci. U.S.A.* **1992**, *89*, 6094−6098.
(12) Prchla, E.; Plank, C.; Wagner, E.; Blaas, D.; Fuchs, R. Virus-Mediated Release of Endosomal Content in Vitro: Different Behavior of Adenovirus and Rhinovirus Serotype 2. *J. Cell. Biol.* **1995**, *131*, 111−123.
(13) Kakudo, T.; Chaki, S.; Futaki, S.; Nakase, I.; Akaji, K.; Kawakami, T.; Maruyama, K.; Kamiya, H.; Harashima, H. Transferrin-Modified Liposomes Equipped with A pH-Sensitive Fusogenic Peptide: An Artificial Viral-Like Delivery System. *Biochemistry.* **2004**, *43*, 5618−5628.
(14) Lorenzi, G. L.; Lee, K. D. Enhanced Plasmid DNA Delivery Using Anionic LPDII by Listeriolysin O Incorporation. *J. Gene Med.* **2005**, *7*, 1077−1085.
(15) Sun, J.; Pohl, E. E.; Krylova, O. O.; Krause, E.; Agapov, I. I.; Tonevitsky, A. G.; Pohl, P. Membrane Destabilization by Ricin. *Eur. Biophys. J.* **2004**, *33*, 572−579.
(16) Meyer, M.; Philipp, A.; Oskuee, R.; Schmidt, C.; Wagner, E. Breathing Life into Polycations: Functionalization with pH-Responsive Endosomolytic Peptides and Polyethylene Glycol Enables siRNA Delivery. *J. Am. Chem. Soc.* **2008**, *130*, 3272−3273.
(17) Boeckle, S.; Fahrmeir, J.; Roedl, W.; Ogris, M.; Wagner, E. Melittin Analogs with High Lytic Activity at Endosomal pH Enhance Transfection with Purified Targeted PEI Polyplexes. *J. Controlled Release* **2006**, *112*, 240−248.
(18) Del Pozo-Rodríguez, A.; Pujals, S.; Delgado, D.; Solinís, M.; Gascón, A.; Giralt, E.; Pedraz, J. A Proline-rich Peptide Improves Cell Transfection of Solid Lipid Nanoparticle-based Non-viral Vectors. *J. Controlled Release* **2009**, *133*, 52−59.
(19) Pack, D. W.; Hoffman, A. S.; Pun, S.; Stayton, P. S. Design and Development of Polymers for Gene Delivery. *Nat. Rev. Drug Discovery.* **2005**, *4*, 581−593.
(20) Mastrobattista, E.; Van Der Aa, M. A.; Hennink, W. E.; Crommelin, D. J. Artificial Viruses: A Nanotechnological Approach to Gene Delivery. *Nat. Rev. Drug Discovery* **2006**, *5*, 115−121.
(21) Boussif, O.; Lezoualc'h, F.; Zanta, M. A.; Mergny, M. D.; Scherman, D.; Demeneix, B.; Behr, J.-P. A Versatile Vector for Gene and Oligonucleotide Transfer into Cells in Culture and in Vivo: Polyethylenimine. *Proc. Natl. Acad. Sci. U. S. A.* **1995**, *92*, 7297−7301.
(22) Lin, C.; Engbersen, J. F. Effect of Chemical Functionalities in Poly(amido amine)s for Non-viral Gene Transfection. *J. Controlled Release* **2008**, *132*, 267−272.
(23) Cheung, C. Y.; Murthy, N.; Stayton, P. S.; Hoffman, A. S. A pH-Sensitive Polymer that Enhances Cationic Lipid-Mediated Gene Transfer. *Bioconjugate Chem.* **2001**, *12*, 906−910.
(24) Mellman, I.; Fuchs, R.; Helenius, A. Acidification of the Endocytic and Exocytic Pathways. *Annu. Rev. Biochem.* **1986**, *55*, 663−700.
(25) Erbacher, P.; Roche, A. C.; Monsigny, M.; Midoux, P. Putative Role of Chloroquine in Gene Transfer into a Human Hepatoma Cell Line by DNA/Lactosylated Polylysine Complexes. *Exp. Cell Res.* **1996**, *225*, 186−194.
(26) Kichler, A.; Leborgne, C.; Danos, O.; Bechinger, B. Characterization of the Gene Transfer Process Mediated by Histidine-Rich Peptides. *J. Mol. Med. (Heidelberg, Ger.).* **2007**, *85*, 191−201.
(27) Nishiyama, N.; Jang, W.-D.; Date, K.; Miyata, K.; Kataoka, K. Photochemical Enhancement of Transgene Expression by Polymeric Micelles Incorporating Plasmid DNA and Dendrimer-based Photosensitizer. *J. Drug Targeting.* **2006**, *14*, 413−424.
(28) Berg, K.; Selbo, P. K.; Prasmickaite, L.; Tjelle, T. E.; Sandvig, K.; Moan, J.; Gaudernack, G.; Fodstad, Ø.; Kjølsrud, S.; Anholt, H. Photochemical Internalization: A Novel Technology for Delivery of Macromolecules into Cytosol. *Cancer Res.* **1999**, *59*, 1180−1183.
(29) Appelqvist, H.; Wäster, P.; Kågedal, K.; Öllinger, K. The Lysosome: From Waste Bag to Potential Therapeutic Target. *J. Mol. Cell Biol. (Oxford, U.K.).* **2013**, *5*, 214−226.
(30) Soleimani, M.; Nadri, S. A Protocol for Isolation and Culture of Mesenchymal Stem Cells from Mouse Bone Marrow. *Nat. Protoc.* **2009**, *4*, 102−106.
(31) Liu, S.; Ma, L.; Tan, R.; Lu, Q.; Geng, Y.; Wang, G.; Gu, Z. Safe and Efficient Local Gene Delivery into Skeletal Muscle via a Combination of Pluronic L64 and Modified Electrotransfer. *Gene Ther.* **2014**, *21*, 558−565.
(32) Khalil, I. A.; Kogure, K.; Akita, H.; Harashima, H. Uptake Pathways and Subsequent Intracellular Trafficking in Nonviral Gene Delivery. *Pharmacol. Rev.* **2006**, *58*, 32−45.
(33) Rejman, J.; Oberle, V.; Zuhorn, I.; Hoekstra, D. Size-Dependent Internalization of Particles Via the Pathways of Clathrin- and Caveolae-Mediated Endocytosis. *Biochem. J.* **2004**, *377*, 159−169.
(34) Rejman, J.; Bragonzi, A.; Conese, M. Role of Clathrin- and Caveolae-Mediated Endocytosis in Gene Transfer Mediated by Lipo- and Polyplexes. *Mol. Ther.* **2005**, *12*, 468−474.
(35) Iversen, T.-G.; Skotland, T.; Sandvig, K. Endocytosis and Intracellular Transport of Nanoparticles: Present Knowledge and Need for Future Studies. *Nano Today.* **2011**, *6*, 176−185.
(36) Sahay, G.; Alakhova, D. Y.; Kabanov, A. V. Endocytosis of Nanomedicines. *J. Controlled Release* **2010**, *145*, 182−195.
(37) Van der Aa, M.; Huth, U.; Häfele, S.; Schubert, R.; Oosting, R.; Mastrobattista, E.; Hennink, W.; Peschka-Süss, R.; Koning, G.; Crommelin, D. Cellular Uptake of Cationic Polymer-DNA Complexes via Caveolae Plays A Pivotal Role in Gene Transfection in COS-7 Cells. *Pharm. Res.* **2007**, *24*, 1590−1598.
(38) Hufnagel, H.; Hakim, P.; Lima, A.; Hollfelder, F. Fluid Phase Endocytosis Contributes to Transfection of DNA by PEI-25. *Mol. Ther.* **2009**, *17*, 1411−1417.
(39) Sriadibhatla, S.; Yang, Z.; Gebhart, C.; Alakhov, V. Y.; Kabanov, A. Transcriptional Activation of Gene Expression by Pluronic Block Copolymers in Stably and Transiently Transfected cells. *Mol. Ther.* **2006**, *13*, 804−813.
(40) Song, H.; Liu, S.; Li, C.; Geng, Y.; Wang, G.; Gu, Z. Pluronic L64-Mediated Stable HIF-1α Expression in Muscle for Therapeutic Angiogenesis in Mouse Hindlimb Ischemia. *Int. J. Nanomed.* **2014**, *9*, 3439−3452.
(41) Yang, Z.; Zhu, J.; Sriadibhatla, S.; Gebhart, C.; Alakhov, V.; Kabanov, A. Promoter- and Strain-Selective Enhancement of Gene Expression in A Mouse Skeletal Muscle by A Polymer Excipient Pluronic P85. *J. Controlled Release* **2005**, *108*, 496−512.

DOI: 10.1021/acsami.5b00486
ACS Appl. Mater. Interfaces 2015, 7, 7282−7293

(42) Kabanov, A. V.; Lemieux, P.; Vinogradov, S.; Alakhov, V. Pluronic® Block Copolymers: Novel Functional Molecules for Gene Therapy. *Adv. Drug Delivery Rev.* **2002**, *54*, 223−233.
(43) Batrakova, E. V.; Kabanov, A. V. Pluronic Block Copolymers: Evolution of Drug Delivery Concept from Inert Nanocarriers to Biological Response Modifiers. *J. Controlled Release* **2008**, *130*, 98−106.
(44) Gau-Racine, J.; Lal, J.; Zeghal, M.; Auvray, L. PEO-PPO Block Copolymer Vectors do not Interact Directly with DNA but with Lipid Membranes. *J. Phys. Chem. B* **2007**, *111*, 9900−9907.
(45) Schulz, M.; Olubummo, A.; Binder, W. H. Beyond the Lipid-Bilayer: Interaction of Polymers and Nanoparticles with Membranes. *Soft Matter.* **2012**, *8*, 4849−4864.
(46) Binder, W. H. Polymer-Induced Transient Pores in Lipid Membranes. *Angew. Chem., Int. Ed.* **2008**, *47*, 3092−3095.
(47) Moghimi, S. M.; Hunter, A. C. Poloxamers and Poloxamines in Nanoparticle Engineering and Experimental Medicine. *Curr. Trends Biotechnol.* **2000**, *18*, 412−420.
(48) Pu, L.; Geng, Y.; Liu, S.; Chen, J.; Luo, K.; Wang, G.; Gu, Z. Electroneutralized Amphiphilic Triblock Copolymer with a Peptide Dendron for Efficient Muscular Gene Delivery. *ACS Appl. Mater. Interfaces.* **2014**, *6*, 15344−15351.

DOI: 10.1021/acsami.5b00486
ACS Appl. Mater. Interfaces 2015, 7, 7282−7293